Available online at www.sciencedirect.com
SCIENCE DIRECT®
Journal of Solid State Chemistry 178 (2005) 3251–3255
JOURNAL OF SOLID STATE CHEMISTRY
www.elsevier.com/locate/jssc

Synthesis, crystal structure, and electronic structure of $RbVSe_2$

Bin Deng[a], Fu Qiang Huang[c], Donald E. Ellis[b], James A. Ibers[a,*]

[a]*Department of Chemistry, Northwestern University, 2145 Sheridan Road, Evanston, Illinois 60208-3113, USA*
[b]*Department of Physics and Astronomy, Northwestern University, 2145 Sheridan Road, Evanston, Illinois 60208-3113, USA*
[c]*Shanghai Institute of Ceramics, Shanghai, 200050, P. R. China*

Received 13 June 2005; received in revised form 26 July 2005; accepted 4 August 2005
Available online 6 September 2005

Abstract

$RbVSe_2$ has been synthesized at 773 K through the reaction of V and Se with a Rb_2Se_3 reactive flux. The compound crystallizes in the orthorhombic space group D_{2h}^{24}-*Fddd* with 16 formula units in a cell of dimensions $a = 5.6724(9)$ Å, $b = 13.648(2)$ Å, and $c = 24.181(4)$ Å at $T = 153$ K. The structure possesses infinite one-dimensional $^1_\infty[VSe_2^-]$ chains of edge-sharing VSe_4 tetrahedra separated from the Rb^+ ions. These $^1_\infty[VSe_2^-]$ chains distort slightly to $^1_\infty[V(1)V(2)Se_4^{2-}]$ chains. The V–V distance within these chains is 2.8362(4) Å. First-principles total energy calculations indicate that a non-magnetic configuration for the V^{3+} cations is the most stable.

Keywords: Rubidium vanadium diselenide; Crystal structure; Synthesis; Electronic structure

1. Introduction

Among one-dimensional vanadium chalcogenides the two compounds $BaVS_3$ and $BaVSe_3$ have been studied extensively owing to their interesting magnetic and electrical properties [1–6]. In these compounds VQ_6 (Q = S or Se) octahedra form one-dimensional $^1_\infty[VQ_3]$ chains by face sharing. Because V can also be tetrahedrally coordinated in metal chalcogenides, we were interested in attempting the synthesis of compounds that might contain one-dimensional chains formed by edge-sharing VQ_4 tetrahedra. Among compounds of the general composition $A_2MM'Q_4$ (A = Na, K, Rb, Cs, Tl; M = Cu, Ag; M' = V, Nb, Ta; Q = S, Se) there is a large subset of isostructural compounds that crystallize in space group *Fddd*. These possess a structure comprising one-dimensional $^1_\infty[MM'Se_4^{2-}]$ chains of edge-sharing MQ_4 and $M'Q_4$ tetrahedra. In this subgroup there are eight V/S or V/Se compounds, namely K_2CuVS_4 [7], Rb_2CuVS_4 [8], K_2CuVSe_4 [8], K_2AgVS_4 [9], Rb_2AgVS_4 [9], Cs_2AgVS_4 [10], K_2AgVSe_4 [8], and Rb_2AgVSe_4 [10]. However, there appear to be no compounds of formula $A_2V_2Q_4$, that is AVQ_2, that crystallize in space group *Fddd*. Such a compound was our target. Here we report the synthesis, structure, and electronic structure of $RbVSe_2$, a compound that crystallizes in space group *Fddd* and possesses infinite one-dimensional chains of edge-sharing VSe_4 tetrahedra.

2. Experimental section

2.1. Synthesis

The following reagents were used as obtained: Rb (Aldrich, 98 + %), V (Strem, 99.5%), and Se (Alfa Aesar, 99.5%). Rb_2Se_3, the reactive flux [11] employed in the synthesis, was prepared by the stoichiometric reaction of the elements in liquid NH_3. $RbVSe_2$ was synthesized by the reaction of 1.0 mmol of V, 2.0 mmol of Se, and 0.5 mmol of Rb_2Se_3. The reaction mixture was loaded into a fused-silica tube under an Ar atmosphere in a glove box. The tube was sealed under

*Corresponding author. Fax: +1 847 491 2976.
E-mail address: ibers@chem.northwestern.edu (J.A. Ibers).

0022-4596/$ - see front matter © 2005 Elsevier Inc. All rights reserved.
doi:10.1016/j.jssc.2005.08.004

a 10^{-4} Torr atmosphere and then placed in a computer-controlled furnace. The sample was heated to 773 K in 10 h, kept at 773 K for 72 h, and then slowly cooled at 4 K/h to 293 K. $RbVSe_2$ crystallized as dark needles or plates in about 10% yield. Analysis of the final product with an EDX-equipped Hitachi S-3500 SEM showed the presence of Rb, V, and Se. The compound is extremely air-sensitive. This air sensitivity has prevented further physical measurements beyond the crystal-structure determination.

2.2. Crystallography

Single-crystal X-ray diffraction data were obtained with the use of graphite-monochromatized Mo$K\alpha$ radiation ($\lambda = 0.71073$ Å) at 153 K on a Bruker Smart-1000 CCD diffractometer [12]. The crystal-to-detector distance was 5.023 cm. Crystal decay was monitored by recollecting 50 initial frames at the end of data collection. Data were collected by a scan of 0.3° in ω in four groups of 606 frames at φ settings of 0°, 90°, 180°, and 270°. The exposure time was 15 s/frame. The collection of the intensity data was carried out with the program SMART [12]. Cell refinement and data reduction were carried out with the use of the program SAINT [12] and face-indexed absorption corrections were performed numerically with the use of the program XPREP [13]. Then the program SADABS [12] was employed to make incident beam and decay corrections.

The structure was solved with the direct methods program SHELXS and refined with the full-matrix least-squares program SHELXL of the SHELXTL suite of programs [13]. The final refinement included anisotropic displacement parameters and a secondary extinction correction. Additional crystallographic details are given in Table 1 and in Section 4. Table 2 presents selected bond distances and bond angles for $RbVSe_2$.

Table 1
Crystal data and experimental details

Formula	$RbVSe_2$
Formula mass	294.33
Space group	D_{2h}^{24}-*Fddd*
a (Å)	5.6724 (9)
b (Å)	13.648 (2)
c (Å)	24.181 (4)
V (Å^3)	1872.0 (5)
T (K)	153
Z	16
ρ_c (g/cm^3)	4.177
μ (cm^{-1})	277.94
$R(F)$[a]	0.0340
$R_w(F_o^2)$[b]	0.0971

[a] $R(F) = \sum||F_o|-|F_c||/\sum|F_o|$ for $F_o^2 > 2\sigma(F_o^2)$.
[b] $R_w\ (F_o^2) = [\sum\ w(F_o^2-F_c^2)^2/\sum\ wF_o^4]^{1/2}$, $w^{-1} = \sigma^2(F_o^2) + (0.06P)^2$ for $F_o^2 \geqslant 0$; $w^{-1} = \sigma^2(F_o^2)$ for $F_o^2 < 0$, where $P = (F_o^2 + 2\ F_c^2)/3$.

Table 2
Selected bond distances (Å) and bond angles (°) for $RbVSe_2$

Rb–Se × 2	3.5162(6)	V1–Se × 4	2.3760(5)
Rb–Se × 2	3.5530(6)	V2–Se × 4	2.3485(5)
Rb–Se × 2	3.5570(8)	V1–V2	2.8362(5)
Rb–Se × 2	3.6957(8)		
Se–V1–Se × 2	111.87(3)	Se–V2–Se × 2	110.37(3)
Se–V1–Se × 2	105.33(2)	Se–V2–Se × 2	107.11(2)
Se–V1–Se × 2	111.29(3)	Se–V2–Se × 2	110.96(3)

2.3. Tight-binding LMTO calculations

In these calculations the TB-LMTO program was used. This is a self-consistent, scalar relativistic linearized muffin-tin orbital program of Andersen and co-workers [14–16] within the atomic sphere approximation. This method splits the crystal space into overlapping atomic spheres (Wigner–Seitz spheres) whose radii are chosen to fill completely the crystal volume. The calculated radii were 4.65, 2.55, 2.61, and 2.59 Bohr for Rb, V1, V2, and Se, respectively. To fill completely the space, six empty spheres were introduced. The positions and radii (2.51, 1.56, 1.63, 1.32, 1.18, and 1.21 Bohr) of these empty spheres were calculated automatically. No more than 16% overlap between any two atom-centered spheres was allowed. The TB-LMTO scheme has the twin virtues of being rapid, and in providing an atomic-orbital related analysis of energy and charge density composition. In the calculations presented here, the von Barth–Hedin exchange-correlation potential was used within the local density approximation [17]. All *k*-space integrations were performed with the tetrahedron method with the use of 280 *k*-points [18,19]. The basis sets consisted of the valence 5*s* electrons for Rb; 3*d* and 4*s* electrons for V; 4*s* and 4*p* electrons for Se; and 1*s* electrons for empty spheres. The 5*p* and 5*d* electrons for Rb, 4*d* electrons for Se, and *p*–*d* states for empty spheres were downfolded by means of the technique described by Löwdin [20]. The crystal orbital Hamiltonian populations (COHP) [21], which are the densities of states (DOS) weighted by the corresponding Hamiltonian matrix elements, provide a useful means of interpreting the V–Se and V–V interactions.

2.4. Full-potential electronic structure calculations

The full-potential LAPW method is a highly accurate approach for determining band structures and carrying out structural relaxation. Its computational cost is much higher than that of the TB-LMTO scheme; therefore, it is best applied selectively. Here we are particularly interested in exploring possible magnetic interactions, and the relative energies of different magnetic states. Full-potential band-structure calculations for $RbVSe_2$

were performed by means of the FP-LAPW method [22,23] as implemented in the WIEN2k code [24]. The exchange and correlation interactions were treated in the generalized gradient approximation within density-functional theory with the use of the parameterization of Perdew and Wang [25]. The muffin-tin radii were chosen as 2.6, 2.1, and 2.3 Bohr for Rb, V, and Se, respectively. The plane-wave expansion cutoffs for wave functions (RK_{max}) and for the densities and potentials (G_{max}) were chosen as 7 and 14 $Bohr^{-1}$, respectively. Brillouin-zone integrations with self-consistency cycles were performed by means of a tetrahedron method [26] with the use of 100 k points throughout the Brillouin zone.

3. Results and discussion

3.1. Synthesis

$RbVSe_2$ was synthesized in about 10% yield by the reaction of V and Se with a Rb_2Se_3 flux at 773 K. The compound is extremely air-sensitive.

3.2. Crystal structure

A projection of the structure of $RbVSe_2$ down [100] is shown in Fig. 1. Selected distances and angles are given in Table 2. The closest Se···Se distance is 3.76 Å; therefore, there are no Se–Se bonds in the structure. Consequently, the formal oxidation states of Rb, V, and Se are 1+, 3+, and 2−, respectively. The structure is composed of one-dimensional $^1_\infty[VSe_2^-]$ chains that run parallel to [100]. The Rb^+ cations, which are eight-coordinated, are well-separated from the chains. Each of the two crystallographically distinct V atoms, V(1) and V(2), has crystallographically imposed 222 symmetry and is tetrahedrally coordinated by four Se atoms. The one-dimensional infinite linear chains comprise the

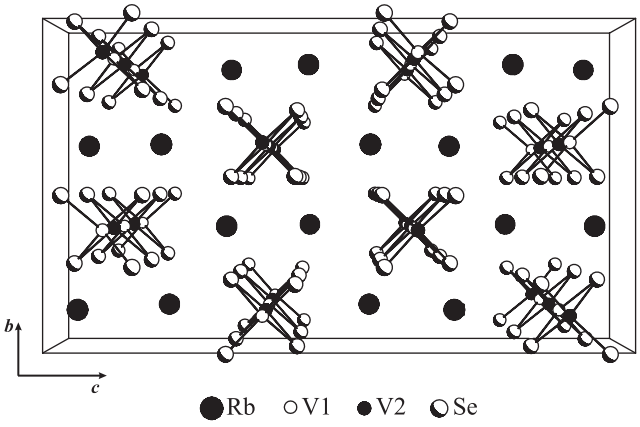

Fig. 1. Unit cell of $RbVSe_2$ viewed down [100].

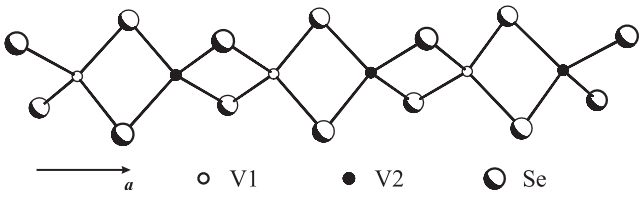

Fig. 2. The $^1_\infty[V(1)V(2)Se_4^{2-}]$ chain in $RbVSe_2$.

sharing of edges by successive $V(1)Se_4$ and $V(2)Se_4$ tetrahedra (Fig. 2) and hence may be written as $^1_\infty[V(1)V(2)Se_4^{2-}]$. The V(1)–Se distance is 2.3760(5) Å and the Se–V(1)–Se angles are 105.33(2)°, 111.29(3)°, and 111.87(3)°; the V(2)–Se distance is 2.3485(5) Å and the Se–V(2)–Se angles are 107.11(2)°, 110.37(3)°, and 110.96(3)°. Compare these to the V–Se distance of 2.312(1) Å and Se–V–Se angles of 107.02(2)–114.14(2)° in Rb_2AgVSe_4 [10]. The edge sharing of the VSe_4 tetrahedra in $RbVSe_2$ leads to a V–V distance of only 2.8362(4) Å, which is comparable to those of 2.8084(3) Å in the non-ferromagnetic phase of $BaVS_3$ [3], 2.8105(4) Å in the ferromagnetic phase of $BaVS_3$ [3], and 2.9310(7) Å in $BaVSe_3$ [6]. The latter phases contain $^1_\infty[VQ_3^{2-}]$ chains formed by face-sharing octahedra.

3.3. Electronic structure

Fig. 3 shows the –COHP curves and their integrals (dashed line) for the V1–Se, V2–Se, and V1–V2 interactions. The COHP values integrated to the Fermi level (ICOHP), which can roughly measure the bond strength, are −2.73 eV for V1–Se, −3.14 eV for V2–Se, and −0.57 eV for V1–V2. This indicates that the V1–V2 bonds are weaker than the V–Se bonds. As shown in Fig. 3, the V–Se bonds are mainly formed in the region from −5 eV to −2 eV. There is also a small V–Se bonding contribution in the region from −14 eV to −12 eV that results from the overlap among Se 4s orbitals, V 4s orbitals, and V 3d orbitals. For V1–V2 bonds, there are two bonding regions in $RbVSe_2$: one is from −5 eV to −2 eV, and the other is from −1 eV to the Fermi level. Note that both V–Se bonds and V1–V2 bonds are formed in the region from −5 eV to −2 eV. Therefore, we may attribute this overlap population to V–Se–V indirect interactions in this region. In the region from −1 eV to the Fermi level, the wavefunctions of V(1) and V(2) overlap directly. According to Fig. 3, there is a direct bonding interaction between the two V^{3+} cations in this region. Because V^{3+} has a $3d^2$ electronic configuration there could be non-magnetic (strong ligand field) or magnetic (crystal field) states on the ions. If the states are magnetic, then the coupling between the two adjacent V1 and V2 ions could be antiferromagnetic or ferromagnetic. Because the extreme air sensitivity of $RbVSe_2$ precluded magnetic measurements, we performed first-principles total

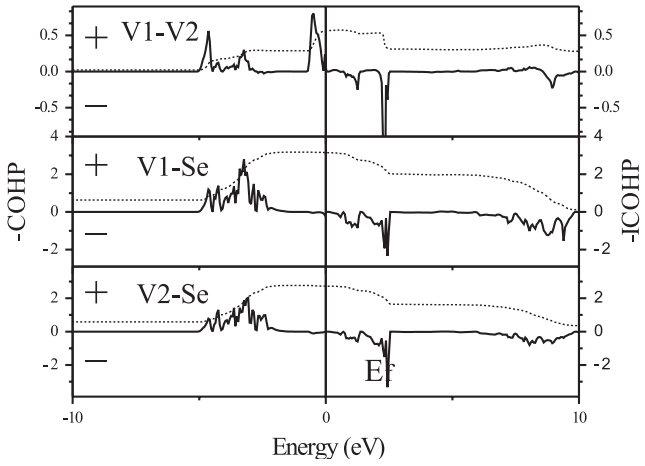

Fig. 3. –COHP curve for the V(1)–V(2), V(1)–Se, and V(2)–Se bonds in $RbVSe_2$.(The dashed line is the integration curve, –ICOHP.)

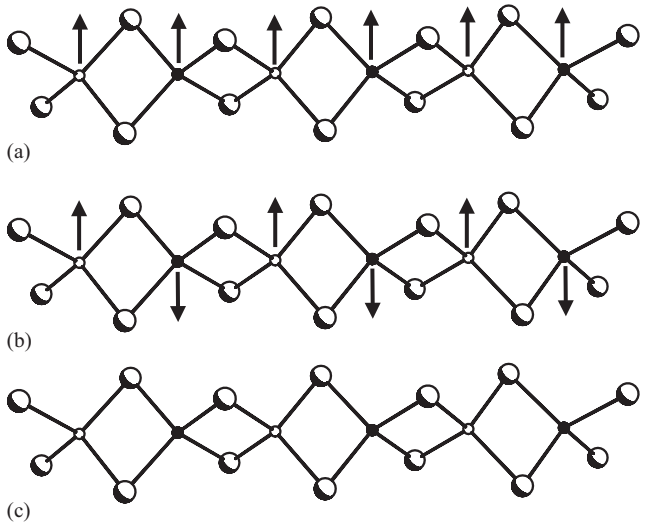

Fig. 4. The simplest magnetic configurations of $RbVSe_2$: ferromagnetic (a), antiferromagnetic (b), and non-magnetic (c).

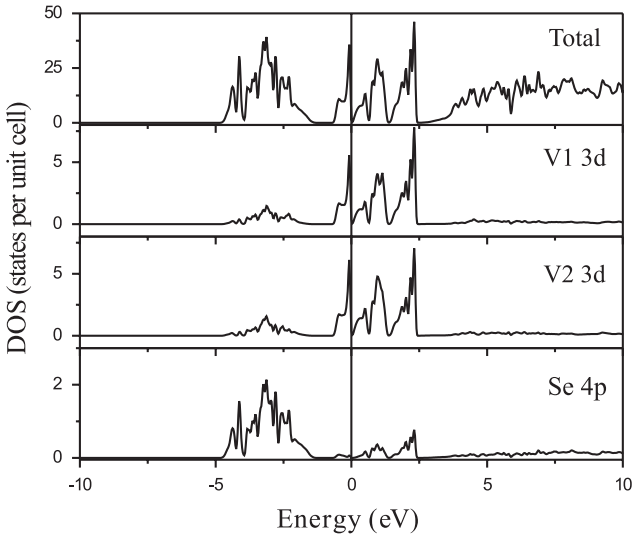

Fig. 5. Total and partial DOS of $RbVSe_2$.

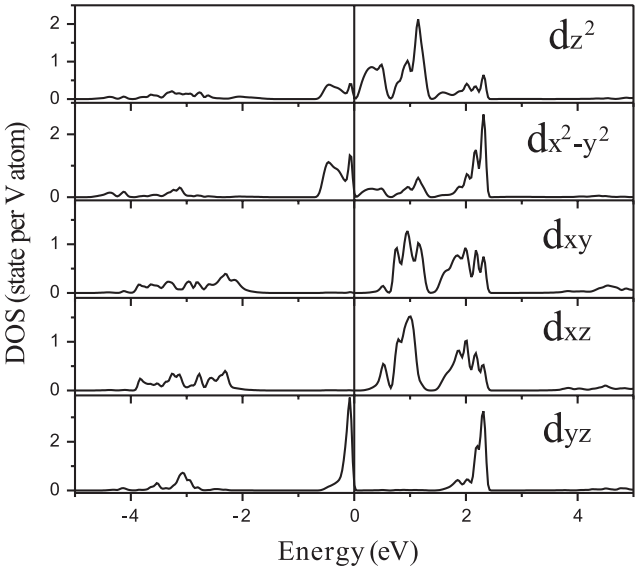

Fig. 6. Partial DOS of the V1 (3*d*) orbitals. The coordinate system for the *d* orbitals relative to the crystal coordinate system is *z* along *a*, *y* along *b*, and *x* along *c*; thus dz^2 is in the chain direction.

energy calculations by both tight-binding and full-potential methods to study the stability of the simplest magnetic configurations. The initial magnetic configurations are indicated in Fig. 4. Both ferromagnetic (Fig. 4(a)) and antiferromagnetic (Fig. 4(b)) configurations are found to be unstable. As self-consistent-field iterations progress the magnetic moments on the V atoms decay towards zero. Thus the non-magnetic configuration (Fig. 4(c)), at least within the simplest models considered here, is the most stable.

The total and selected partial DOS of $RbVSe_2$, shown in Figs. 5 and 6, were obtained from LAPW calculations. Because the partial DOS of V2 are similar to those of V1 we show only the latter in Fig. 6. Most of the contributions around the Fermi level are from V 3*d* and Se 4*p* orbitals. Because Rb makes almost no contributions to the DOS, the electronic properties are essentially determined by the one-dimensional $^1_\infty[V(1)V(2)Se_4^{2-}]$ chains along [100]. The V and Se orbitals are hybridized around the Fermi level, as can be seen from the overlap among them. The Se 4*p* orbitals are mainly located in the region from −5 eV to −1 eV below the Fermi level. All five *d* orbitals also contribute in this region where V–Se bonds are formed. In the region from −1 eV to the Fermi level, we see important contributions from the dz^2, dx^2-y^2, and d*yz* orbitals. Because the V–V bonds are formed in this region and the $^1_\infty[V(1)V(2)Se_4^{2-}]$ chains are along the [100] axis the V–V bonds are mainly π in character. The d*xz* and d*xy* sub-bands are mainly

located in the region from +0.5 eV to +2.5 eV above the Fermi level and the region from −4 eV to −2 eV below the Fermi level. The partial occupancies determined by charge integration with the muffin-tin spheres are 0.374 for dz^2, 0.697 for dx^2-y^2, 0.857 for dyz, 0.381 for dxz, and 0.401 for dxy. For the V2 muffin-tin sphere, these occupancies are 0.362 for dz^2, 0.724 for dx^2-y^2, 0.885 for dyz, 0.365 for dxz, and 0.361 for dxy. The net 3d occupancy of 2.71e$^-$ and 2.70e$^-$ for V1 and V2, respectively, reflects the V–Se covalent bonding contributions in addition to the nominal crystal-field populations.

4. Supporting information

The crystallographic file in cif format for $RbVSe_2$ has been deposited with FIZ Karlsruhe as CSD number 415479. The data may be obtained free of charge by contacting FIZ Karlsruhe at +49 7247 808 666 (fax) or crysdata@fiz–karlsruhe.de (email).

Acknowledgments

This research was supported in part by US National Science Foundation Grant DMR00-96676 and the MRSEC program of the US National Science Foundation (DMR00-76097) at the Materials Research Center of Northwestern University. F.Q.H. acknowledges support from National Science Foundation of China Grant B010504-20471068.

References

[1] M. Nakamura, A. Sekiyama, H. Namatame, A. Fujimori, H. Yoshihara, T. Ohtani, A. Misu, M. Takano, Phys. Rev. B 49 (1994) 16191–16201.
[2] M. Ghedira, J. Chenavas, F. Sayetat, M. Marezio, O. Massenet, J. Mercier, Acta Crystallogr. Sect. B: Struct. Crystallogr. Cryst. Chem. 37 (1981) 1491–1496.
[3] J. Kelber, J.D. Jorgensen, M.H. Mueller, Acta Crystallogr. Sect. B: Struct. Crystallogr. Cryst. Chem. 35 (1979) 2473–2475.
[4] P. Fazekas, K. Penc, H. Berger, L. Forró, S. Csonka, I. Kézsmárki, G. Mihály, Physica B 312–313 (2002) 694–695.
[5] I. Kézsmárki, S. Csonka, H. Berger, L. Forró, P. Fazekas, G. Mihály, Phys. Rev. B 63 (2001) 811061–811064.
[6] J. Kelber, A.H. Reis Jr, A.T. Aldred, M.H. Mueller, O. Massenet, G. DePasquali, G. Stucky, J. Solid State Chem. 30 (1979) 357–364.
[7] P. Dürichen, W. Bensch, Eur. J. Solid State Inorg. Chem. 33 (1996) 309–320.
[8] C. Rumpf, R. Tillinski, C. Näther, P. Dürichen, I. Jeβ, W. Bensch, Eur. J. Solid State Inorg. Chem. 34 (1997) 1187–1198.
[9] W. Bensch, P. Dürichen, Chem. Ber. 129 (1996) 1207–1210.
[10] R. Tillinski, C. Rumpf, C. Näther, P. Dürichen, I. Jeβ, S.A. Schunk, W. Bensch, Z. Anorg. Allg. Chem. 624 (1998) 1285–1290.
[11] S.A. Sunshine, D. Kang, J.A. Ibers, J. Am. Chem. Soc. 109 (1987) 6202–6204.
[12] Bruker, SMART Version 5.054 Data Collection and SAINT-Plus Version 6.45a Data Processing Software for the SMART System, Bruker Analytical X-ray Instruments, Inc., Madison, WI, USA, 2003.
[13] G.M. Sheldrick, SHELXTL Version 6.14, Bruker Analytical X-ray Instruments, Inc., Madison, WI, USA, 2003.
[14] O.K. Andersen, Phys. Rev. B 12 (1975) 3060–3083.
[15] O.K. Andersen, O. Jepsen, Phys. Rev. Lett. 53 (1984) 2571–2574.
[16] O. Jepsen, O.K. Andersen, Z. Phys. B: Condens. Matter 97 (1995) 35–47.
[17] L. Hedin, B.I. Lundqvist, J. Phys. Chem. Solids 4 (1971) 2064–2083.
[18] W.R.L. Lambrecht, O.K. Andersen, Phys. Rev. B 34 (1986) 2439–2449.
[19] O. Jepsen, O.K. Andersen, Solid State Commun. 9 (1971) 1763–1767.
[20] P.-O. Löwdin, J. Chem. Phys. 19 (1951) 1396–1401.
[21] R. Dronskowski, P.E. Blöchl, J. Phys. Chem. 97 (1993) 8617–8624.
[22] E. Wimmer, H. Krakauer, M. Weinert, A.J. Freeman, Phys. Rev. B 24 (1981) 864–875.
[23] M. Weinert, E. Wimmer, A.J. Freeman, Phys. Rev. B 26 (1982) 4571–4578.
[24] P. Blaha, K. Schwarz, G.K. Madsen, D. Kvasnicka, J. Luitz, WIEN2k. An Augmented Plane Wave + Local Orbitals Program for Calculating Crystal Properties, Karlheinz Schwarz, Techn. Universität Wien, Austria, Vienna, 2001.
[25] J.P. Perdew, Y. Wang, Phys. Rev. B: Condens. Matter 45 (1992) 13244–13249.
[26] P.E. Blöchl, O. Jepsen, O.K. Andersen, Phys. Rev. B: Condens. Matter 49 (1994) 16223–16233.